Catalysis Today 434 (2024) 114674

Contents lists available at ScienceDirect

Catalysis Today

journal homepage: www.elsevier.com/locate/cattod

Use of graphitic carbon nitrides as solar-light-driven photocatalysts for the reduction of p-nitrobenzoic acid

R.López Timoner [a], A. Arques [a,*], A.M. Amat [a], J. Plaza [b], A. Arencibia [c], M.J. López-Muñoz [b,d,**]

[a] Grupo de Procesos de Oxidación Avanzada, Departamento de Ingeniería Textil y Papelera, Universitat Politècnica de València, Campus de Alcoy, Alcoy, Spain
[b] Departamento de Tecnología Química y Ambiental, ESCET, Universidad Rey Juan, Carlos, Móstoles, Spain
[c] Departamento de Tecnología Química, Energética y Mecánica, ESCET, Universidad Rey Juan Carlos, Móstoles, Spain
[d] Instituto de Tecnologías para la Sostenibilidad. Universidad Rey Juan Carlos C/ Tulipán s/n, 28933, Móstoles, España

ARTICLE INFO

Keywords:
Reduction
Photocatalysis
Graphitic carbon nitrides
P-nitrobenzoic acid

ABSTRACT

The use of graphitic carbon nitrides (g-C_3N_4) as photocatalysts for the reduction of p-nitrobenzoic acid (PNBA) under simulated sunlight has been investigated. The photocatalysts were synthesized through the thermal polymerization of melamine and urea. The effects of the g-C_3N_4 precursor employed in the synthesis, the thermal exfoliation treatment, the addition of sacrificial agents, and the pH conditions were evaluated. It was found that the presence of carboxylic acids as sacrificial electron donors was required to attain the photocatalytic reduction of PNBA, while amines or alcohols did not lead to any activity for this purpose. Furthermore, it was observed that the precursor used in the synthesis of graphitic carbon nitride had a slight influence on the photocatalytic activity, whereas the thermal treatment of the bulk g-C_3N_4 materials exhibited a favourable effect. The best results were obtained upon addition of oxalic acid at pH = 3 using the carbon nitride exfoliated materials, achieving in these conditions the complete removal of PNBA after ca. 60 min of irradiation. Time resolved profiles of p-aminobenzoic acid (PABA) agree with an initial reduction of PNBA to form this compound, followed by oxidation of PABA by reactive oxygen species formed in the reaction medium.

1. Introduction

Wastewater decontamination has received attention from researchers for many decades. This has led to the development of trains of processes implemented in wastewater treatment plants (WWTP), which are generally very efficient in the decontamination of urban effluents. However, the nature of the pollutants found in the inlet effluent of WWTPs is very wide and some of the incoming chemicals are refractory to conventional treatments. The difficulty of removing them has become a major environmental concern since, although in very small concentrations, they are continuously released to the water bodies. Therefore, alternative processes are needed, either as a pretreatment to decrease toxicity or to enhance biodegradability [1,2], or as a post-treatment to refine the quality of WWTP effluents [3,4].

Interestingly, advanced oxidation processes (AOP) have proven to be very efficient to attain the complete degradation of a great number of refractory compounds [5,6], and thus, they are good candidates to be implemented as tertiary or quaternary treatments. Nonetheless, some functional groups of the pollutants are difficult to oxidize, which makes AOPs inefficient for treating substances such as sulphones, halogenated or nitroaromatic compounds which, however, can be more easily reduced. In such cases, it may be worth using reductive processes which, despite being less studied than oxidizing ones, have proven their efficiency for wastewater treatment in niche scenarios. As an example, the reduction of nitroaromatic compounds [7], the dechlorination of chlorophenols [8], or the reduction of heavy metal ions to less harmful species [9] have been successfully achieved by reductive processes, including the use of zero valent iron (ZVI) [7,8,10,11] and semiconductor-mediated photocatalysis [9].

Among the semiconductors that can be employed as photocatalysts in reductive processes, graphitic carbon nitride (g-C_3N_4) has gained significant attention in recent years as a green and low-cost photocatalyst due to its facile preparation from cheap precursors, remarkable stability, controllable structure, and excellent performance under visible light irradiation, attributed to its moderate bandgap of approximately 2.7 eV [12,13]. For reduction processes, g-C_3N_4 materials hold a

* Corresponding author.
** Corresponding author at: Departamento de Tecnología Química y Ambiental, ESCET, Universidad Rey Juan, Carlos, Móstoles, Spain.
E-mail addresses: aarques@txp.upv.es (A. Arques), mariajose.lopez@urjc.es (M.J. López-Muñoz).

https://doi.org/10.1016/j.cattod.2024.114674
Received 27 November 2023; Received in revised form 8 March 2024; Accepted 25 March 2024
Available online 27 March 2024

significant interest due to their favourable conduction band (CB) edge position (~ −1.5 V vs. NHE), which is more negative than the reduction potential of many target pollutants. Thus, photogenerated electrons of g-C_3N_4 can participate in reduction reactions, such as hydrogen production [14], carbon dioxide reduction [15], and reduction of heavy metal species [16]. Nevertheless, most publications have primarily focused on hydrogen production, while their utilization in water decontamination remains relatively underexplored [17].

With this background, the aim of this work is to test the performance of g-C_3N_4 as photocatalyst able to drive reductive processes to deal with chemicals that are reluctant to chemical oxidation. This step is required before real application of g-C_3N_4 can be explored, and niche scenarios can be identified. Here, materials obtained from two precursors (melamine and urea) have been studied as photocatalysts, as well as the effect of exfoliation on their performance. Simulated sunlight has been used as irradiation source and conditions in which photo-reduction can occur have been determined (e.g. pH, presence of oxygen or effect of sacrificial electron donors). In order to perform these experiments, p-nitrobenzoic acid (PNBA) has been chosen as target contaminant as it is recalcitrant vs. conventional chemical oxidative methods; furthermore, it has been described to form p-aminobenzoic acid (PABA) as major reduction product, what allows to identify the presence of reductive steps [8].

2. Material and methods

2.1. Reagents and chemicals

Ultrapure urea and melamine, utilized as precursors for g-C_3N_4, were obtained from Scharlau and Sigma-Aldrich, respectively. High purity PNBA and PABA acid were purchased from Sigma-Aldrich. Formic acid, acetonitrile, methanol (all three HPLC grade), dimethylamine, oxalic acid and citric acid were supplied by PanReac AppliChem. High purity synthetic air and nitrogen were supplied by Praxair.

2.2. Preparation of g-C_3N_4 photocatalyst

The pristine bulk g-C_3N_4 samples, namely PCN-U and PCN-M were synthesized through thermal polymerization using urea and melamine as precursors, respectively. For obtaining PCN-U, 15 g of urea were dissolved in 20 mL of Milli-Q® water and the solution was subjected to a two-step heating process in a muffle furnace. First, it was heated to 400 °C and kept for 2 h at this temperature. Then, temperature was increased to 450 °C, maintained for 2 h and cooled down to room temperature. For obtaining PCN-M, 18 g of melamine were submitted to a similar two-step heating treatment at 520 ºC (2 h) and 540 ºC (2 h). In all cases, the heating rate was set at 5 °C min^{-1}. The exfoliation of the pristine samples was carried out through thermal etching under an air atmosphere at 450 °C (PCN-U) and 500 ºC (PCN-M), obtaining ECN-U and ECN-M materials, respectively.

2.3. Materials characterization

The crystalline phases were characterized using an X-Ray Diffraction (XRD) instrument (Philips X-PERT MPD) with CuKα radiation (λ =1.5418 Å). N_2 adsorption–desorption isotherms were collected at 77 K using a Micromeritics Tristar 3000, where the samples were outgassed at 200 °C for 5 h prior to the analysis. BET surface area (S_{BET}) was calculated in the relative pressure range between 0.05 and 0.2. The structure of the synthesised catalysts was evaluated by scanning electron microscopy (SEM) with a Nova Nano SEM230 instrument. UV–vis diffuse reflectance spectra (UV-DRS) were obtained using a Varian Cary 500 Scan UV-Vis-NIR spectrophotometer. The energy band gap values were obtained by extrapolating a linear fitting in the Tauc plot $((F(R)\ h\cdot\upsilon)^{1/2}$ vs. $h\cdot\upsilon)$. Photoluminescence spectra were acquired by means of a Cary Eclipse spectrophotometer at an excitation wavelength of 350 nm.

2.4. Reaction conditions

PNBA solutions in the range 0.5–1 mg L^{-1} (corresponding to 3.0–6.0 μM) were prepared in Milli-Q® water. Then, the selected g-C_3N_4 photocatalyst was added to the solution in the desired amount (100 – 150 mg L^{-1}) and sonicated for 10 min. Finally, the sacrificial agents (10 mM) were added and, when required, the mixture was deoxygenated by bubbling nitrogen. When needed, pH was modified by dropwise addition of HCl (0.1 M) or NaOH (0.1 M).

Experiments involving simulated solar irradiation were carried out in a glass reactor with a capacity of 250 mL and 8 cm in diameter sealed on the top by a glass filter, which has been described in detail elsewhere [18]. The sample was irradiated by means of a solar simulator (Oriel Instruments, 450 W) emitting collimated light whose spectrum closely matches that of solar spectrum; the glass filter cut off photons with $\lambda <$ 300 nm. For each experiment, the reactor was loaded with 250 mL of the solution to be treated. Magnetic stirring was kept at 550 rpm all along the process.

Experiments with UVC irradiation were carried out in a closed glass reactor (8 cm diameter, 25 cm height). The light source used was a 15 W low-pressure mercury lamp (Heraeus Noblelight) emitting nearly monochromatic irradiation at 254 nm, which was placed axially in the reactor, protected by a quartz envelope. The system was refrigerated by means of an outer water jacket [19]. For each experiment, the reactor was loaded with 500 mL of the solution to be treated. Magnetic stirring was kept all along the process.

2.5. Chemical analysis

Samples were periodically taken from the reactor and flown through polyamide filters (pore diameter of 0.45 μm), purchased from Macherey-Nagel. Concentrations of PNBA and PABA were monitored by HPLC (Hitachi Chromaster chromatograph; VWR) equipped with a UV-Vis detector. A Prevail Hichrom column (C18-Select; 250×4.6 mm; 5 μm) was employed as stationary phase. The eluent consisted in an isocratic mixture of formic acid (60%) and acetonitrile (40%) at a flow rate of 1 mL min^{-1}. Identification and quantitation of target molecules were performed by comparison with standards at a fixed wavelength of 265 nm.

3. Results and discussion

3.1. Characterization of the photocatalysts

Fig. 1 displays the XRD patterns of the synthesised materials. All of them exhibit two characteristic peaks associated with the carbon nitride structure. The first peak is observed at a diffraction angle of $2\theta = 13.2°$ and can be attributed to the (1 0 0) plane. This peak is linked to the presence of hydrogen bonds that connect the structural heptazine units within the 2D plane. The second peak, located at $2\theta = 27.3°$, corresponds to the (0 0 2) plane and is associated with van der Waals forces that result in the periodic stacking of layers along the c-axis [20]. Upon thermal exfoliation of the bulk material, a decrease in the intensity of both peaks is observed, indicative of de-packaging and structural changes [21]. Additionally, in the case of exfoliated melamine-derived materials, a noticeable shift in the diffraction peak to a higher angle was observed. This shift indicates a reduction in the internal distance between stacked adjacent sheets, which can be attributed to the significant planarization of carbon nitride nanosheets during the thermal exfoliation process [22].

The morphological changes induced by the thermal exfoliation treatment were examined using SEM (Fig. 2). A distinct morphology is observed, depending on the precursor utilized. The material derived from melamine (Fig. 2a) exhibits a more laminar and compact structure than PCN-U, which displays irregularly curved layers (Fig. 2b). The thermal treatment of PCN-M induced a decrease in the aggregation of

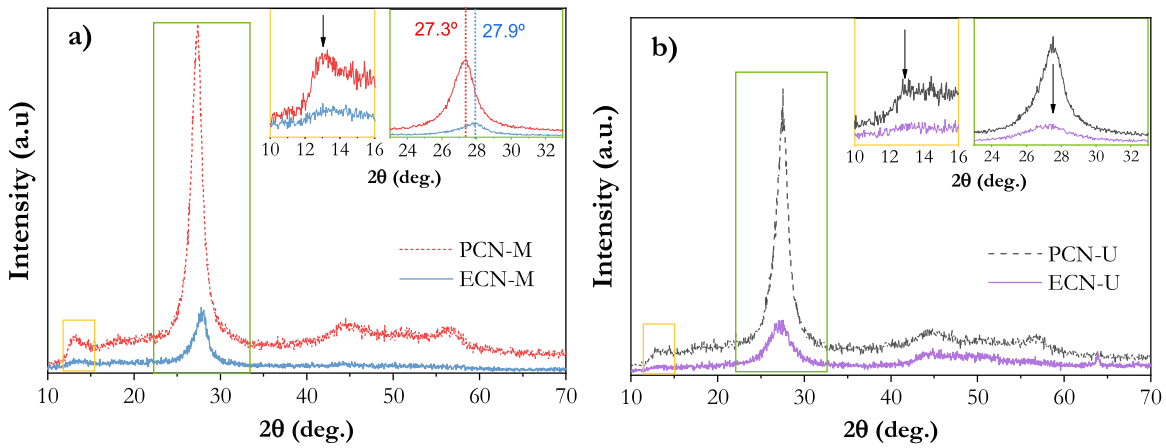

Fig. 1. XRD patterns and enlarged view of the (1 0 0) and (0 0 2) peaks of pristine and exfoliated g-C_3N_4 materials obtained from (a) melamine and (b) urea.

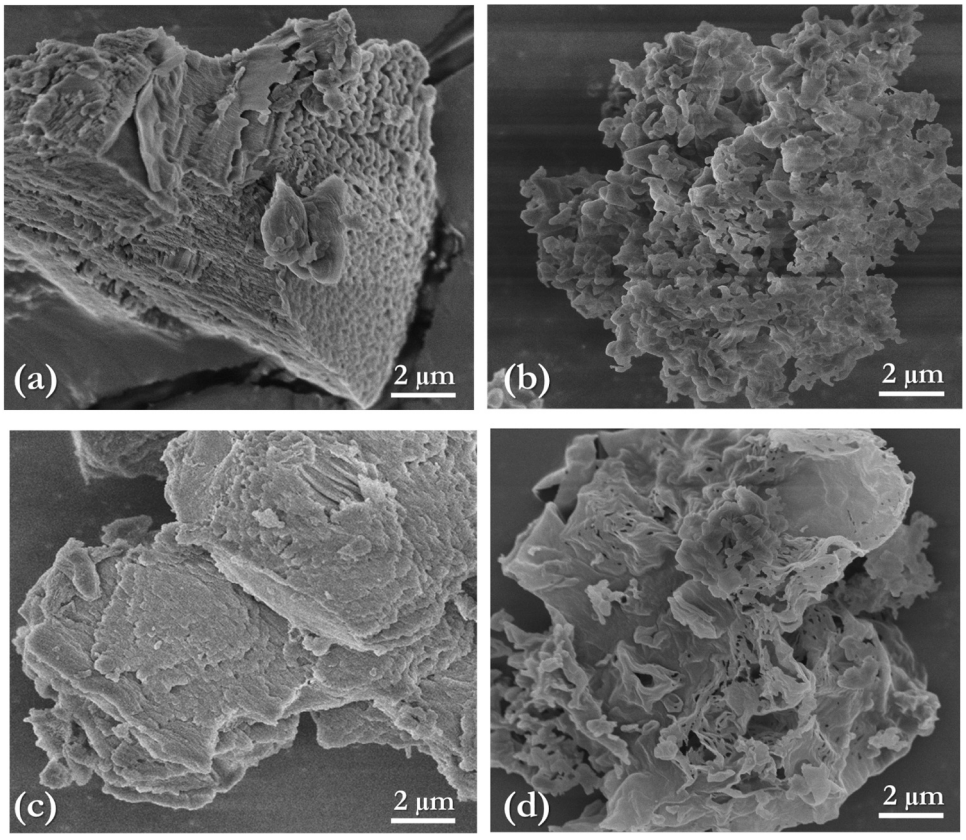

Fig. 2. SEM images of carbon nitride materials: (a) PCN-M, (b) PCN-U, (c) ECN-M, and (d) ECN-U.

the layers and an enhancement in the layer planarity (Fig. 2c) [21]. Conversely, the material obtained from the exfoliation of PCN-U (Fig. 2d) exhibits a porous and disordered structure [23].

The N_2 adsorption-desorption isotherms (Fig. 3) reveal significant changes induced by the thermal treatment of bulk samples. As can be observed, both PCN-M and PCN-U samples display a type III isotherm, which shifts to type IV after their thermal exfoliation. This transformation is accompanied by increased adsorption at moderately high pressures and the presence of an H3-type hysteresis loop, indicating notable alterations in the pore structure and the adsorption behaviour. This is consistent with the substantial increase of both the BET surface area values of the exfoliated materials compared to the bulk samples, from 8 (PCN-M) to 77 $m^2\ g^{-1}$ (ECN-M), and from 42 (PCN-U) to 448 $m^2\ g^{-1}$ (ECN-U), and the pore volumes, which vary from 0.020 (PCN-M) to 0.178 $cm^3\ g^{-1}$ (ECN-M), and from 0.063 (PCN-U) to 0.910 $cm^3\ g^{-1}$ (ECN-U) (Table 1).

To investigate the photoelectric properties of the photocatalysts, UV-Vis diffuse reflectance spectroscopy (UV-Vis DRS) and photoluminescence (PL) measurements were conducted, as depicted in Fig. 3 and Fig. 4, respectively. A comparative analysis between the two bulk materials reveals a significant shift in the absorption threshold of PCN-M towards lower energy regions compared to PCN-U (band gap values shown in Table 1). After the thermal exfoliation process, a slight increase in the bandgap value is observed in ECN-M and ECN-U compared to their respective counterpart pristine bulks, indicative of the quantum confinement effect resulting from a successful exfoliation. This finding

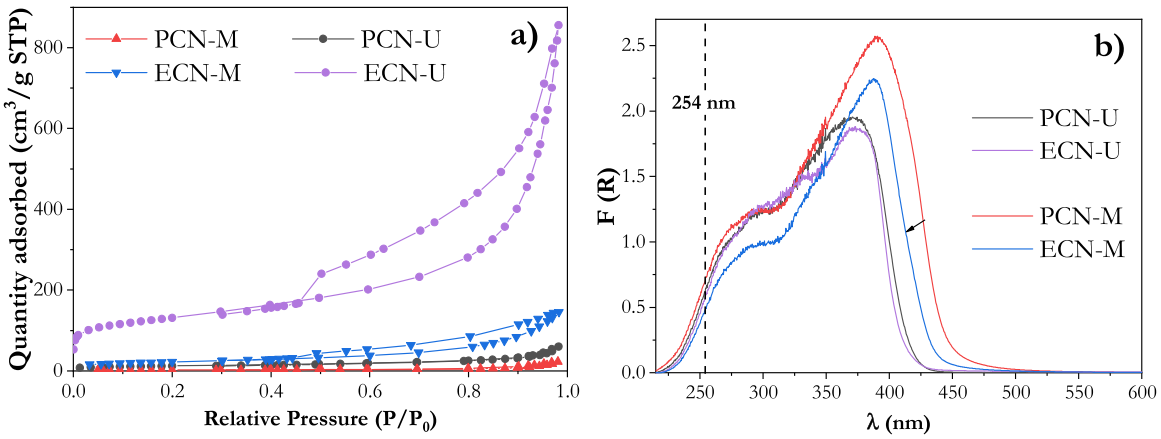

Fig. 3. (a) N_2 adsorption–desorption isotherms at 77 K and (b) UV-Vis DR spectra of the synthesised g-C_3N_4 materials.

Table 1
Summary of the textural and optical properties of the samples.

Samples	S_{BET} (m^2 g^{-1})	V_{pore} (cm^3 g^{-1})	Absorption edge (nm)	Eg (eV)	λ_{max} PL spectra (nm)
PCN-M	8	0.020	545	2.70	460
ECN-M	77	0.178	510	2.75	460
PCN-U	42	0.063	480	2.86	436
ECN-U	448	0.910	475	2.90	436

aligns with previous reports by other researchers [21,24].

The analysis of PL spectra (Fig. 4) revealed a significant reduction in the emission peak intensity when comparing the PCN-M and PCN-U with their exfoliated counterparts. The diminished intensity indicates a marked decrease in the charge carrier recombination after the thermal exfoliation. Furthermore, it is interesting to notice that the maximum intensity emission peak varies with the precursor, being centred at 460 nm in the melamine-derived materials and at 436 nm in the urea-derived samples. Gaussian fitting of the photoluminescence profile was conducted to identify the contributing components. For melamine-derived materials, three primary bands were identified at approximately 439, 460, and 495 nm, consistent with earlier research that associates them with transitions involving the sp^3 C-N σ band, the sp^2 C-N π band, and the lone pair (LP) states of the bridge nitride atom. Specifically, the related transitions would be σ*-LP, π*-LP, and π*-π, respectively [25]. Similarly, for urea-derived materials, three primary bands were also detected, albeit shifted by approximately 15 nm towards the blue side, in line with the 0.2 eV larger bandgap [26].

3.2. Photo-assisted PNBA degradation

Experiments were also performed in the presence of g-C_3N_4, in particular the PCN-U sample. Dark controls resulted in no decrease of PNBA concentration, what allows to dismiss a significant adsorption of the pollutant onto the carbon nitride. Photolysis of PNBA under UVC resulted in pollutant removal in both aerated and deaerated media. (Fig. S1). It has been described that under UVC irradiation, nitrobenzoic acids can undergo scission of ·OH radicals from the carboxylic moieties, which results in a decrease in the concentration of PNBA and the generation of oxidizing species (·OH) [27]. This process occurs from the excited state of the substrate, whose formation only depends on the absorption of photons and thus oxygen does not play a role in this primary step. In agreement, very similar results were observed in the experiments carried out with and without O_2 (Fig.S1) [27]. PCN-U played a negative role, which is characteristic of processes where direct photolysis is predominant. The shielding effect of the photocatalyst particles present in the solution leads to a decrease in the number of photons reaching the target molecules, and the consequent detrimental effect on the photolysis process is not compensated by the potential photocatalytic performance of g-C_3N_4 [28].

On the other hand, irradiation with simulated sunlight (λ > 300 nm) resulted in no photolysis of PNBA, in agreement with the negligible light absorption of this substrate in this region of the spectrum. Also, in the presence of PCN-U, PNBA concentration remained constant (Fig. S1) which indicates that the g-C_3N_4 carbon nitride photocatalyst is not active under these experimental conditions.

Despite this result, the reduction of PNBA by g-C_3N_4 is thermodynamically feasible as the standard potential of the conduction band of the semiconductor is ca. −1.5 V *vs.* NHE [29], and the redox potential for PNBA is ca. −0.4 V *vs.* NHE [30]. However, the conjugated anodic reaction is the oxidation of water, which is a very slow process. As a consequence, the recombination of the photogenerated e^--h^+ pairs is favoured, hence resulting in the observed negligible photocatalytic reduction of PNBA under solar simulated radiation. This drawback could be overcome by the addition of sacrificial agents that are able to act as electron donors to deal with the holes that are formed in the valence band.

Five compounds, namely dimethylamine, methanol, formic acid, citric acid, and oxalic acid were evaluated as sacrificial electron donors in the photocatalytic reduction of PNBA with PCN-U. They were chosen because they are simple molecules which contain functional groups that are commonly used for this purpose (e.g. hydroxyl, amine or carboxylic). The scavengers were added at an initial concentration of 10 mM in N_2-saturated medium. Fig. 5 shows that neither dimethylamine nor methanol were able to promote the reduction of PNBA, while a significant removal of the target pollutant was reached in the presence of the three carboxylic acids. A different mechanism for trapping the photogenerated holes can account for the distinctive behaviour of the scavengers evaluated and the better performance of carboxylic compounds. It has been reported that the photogenerated holes can be trapped either directly by the scavenger, or indirectly through the reaction between HO· and the scavenger. The first mechanism takes place preferentially with chemisorbed organic scavengers, such as carboxylates, whereas the second mechanism occurs with molecules weakly adsorbed or non-adsorbed molecules as it is the case of alcohols [9,31]. Since the valence band potential of g-C_3N_4 is ca. 1.4 V *vs.* NHE., the formation of HO· is unlikely and hence the indirect trap of the hole, what would explain the negligible influence on the photocatalytic reduction of PNBA observed upon addition of methanol and dimethylamine. By contrast, the direct capture of the photogenerated holes by carboxylic acids is favoured. This results in a decreased recombination of photogenerated charges as well as the formation of carboxylic radicals ($CO_2^{\bullet-}$) (equation 1), which are in turn excellent electron donors ($E_0 \approx -1.96$ V *vs.* NHE),

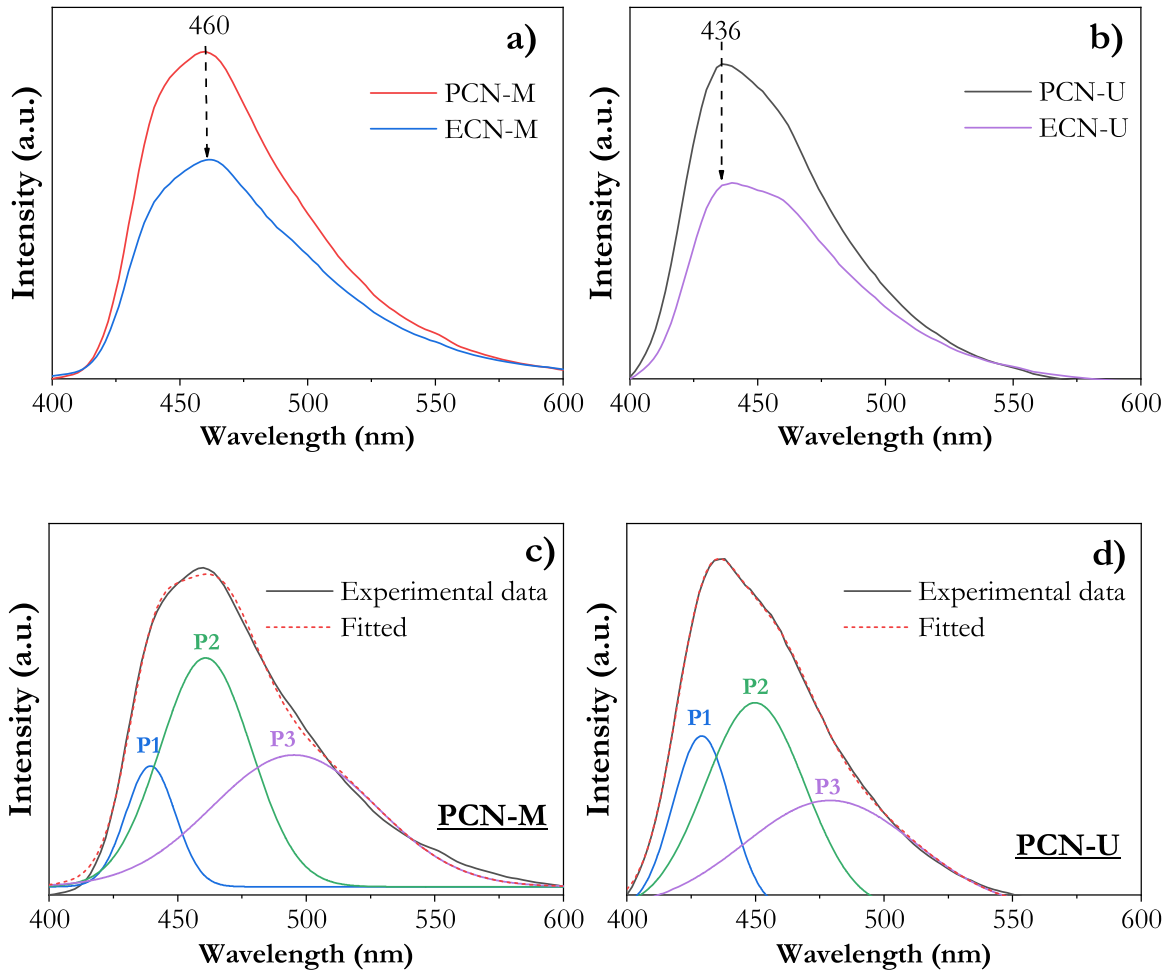

Fig. 4. PL spectra of g-C_3N_4 materials derived from (a) melamine and (b) urea, and (c, d) their profile analysis by Gaussian fitting, respectively.

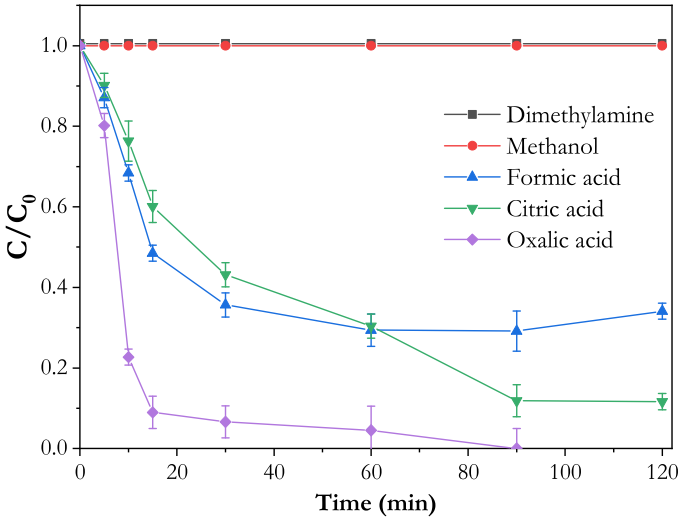

Fig. 5. Plot of the relative concentration profiles of PNBA with irradiation time. Experimental conditions: $[PNBA]_0 = 0.5$ mg L^{-1}; $C_{PCN-U} = 100$ mg L^{-1}; pH = 3; $[S.A.]_0 = 10$ mM; and simulated solar irradiation.

thereby enhancing the PNBA photocatalytic reduction rate [32,33].

$$O_2C\text{-}CO_2^- \rightarrow CO_2 + CO_2^- + e^- \quad (1)$$

The effect of pH on the performance of the carboxylic acids as sacrificial agents in the photocatalytic reduction of PNBA was analysed. Fig. 6 shows that the best results were reached in all cases at pH = 3, where a significant reduction of PNBA concentration was found for every single acid. For all the other tested conditions, the extent of the PNBA degradation was minimal, but when oxalic acid was used at pH = 1. As pointed above, the adsorption of the sacrificial donor is a key step in the scavenging process. Accordingly, the differences observed with pH and between the evaluated acids can be explained based on the point of zero charge (PZC) of g-C_3N_4, (ca. 4.2) [32], and the pKa values of formic acid (3.77), oxalic acid (1.27 and 3.8), citric acid (3.15, 4.77 and 6.40), and PNBA (3.41) [33]. Below the PZC, the surface of the catalyst is positively charged, favouring the approach of negatively charged species, while above its respective pKa, negatively charged carboxylates are predominating. Thus, the optimum pH range is expected to be between the first pKa of the acids and the PZC of the material. Interestingly, pH = 3 is within this range (for oxalic acid) or close to it (in particular for citric acid); this might also explain the trend in PNBA reduction at this pH, which was oxalic acid > citric acid > formic acid. On the other hand, pH =1 is only close to the predicted optimum range for oxalic acid and, in fact, it is the only one able to induce some PNBA removal. Finally, above PZC, the catalyst surface is negatively charged, as well as electron donors and PNBA, thus explaining the scarce PNBA removal in experiments performed at pH ≥ 5.

Finally, the effect of the precursor used for the synthesis of bulk g-C_3N_4 samples, *i.e.*, urea and melamine, and the influence of the subsequent exfoliation treatment was investigated by comparing the photocatalytic performance of PCN-U, PCN-M, ECN-U and ECN-M for PNBA reduction. The reactions were carried out by adding 100 mg L^{-1} of the

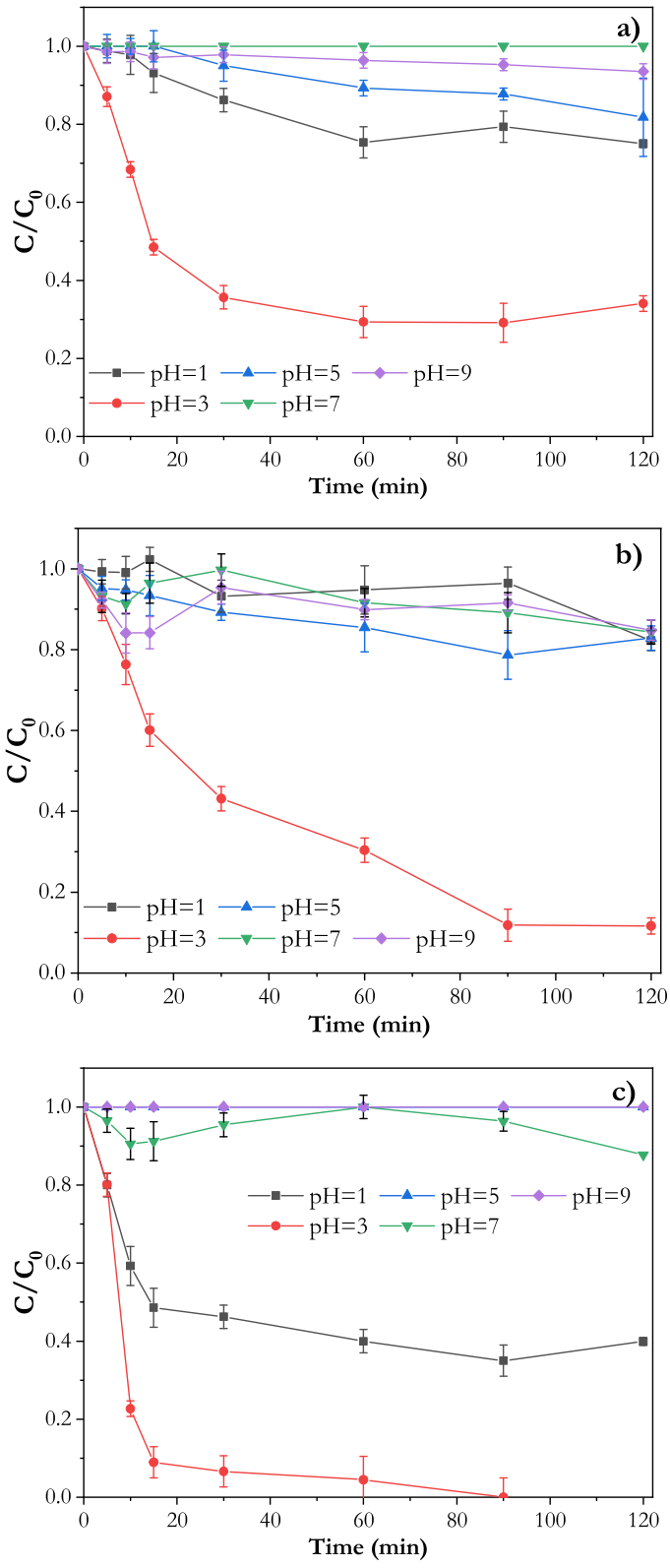

Fig. 6. Plot of the relative concentration of PNBA with irradiation time in the presence of formic acid (a), citric acid (b), and oxalic acid (c) at different pH. Experimental conditions: $[PNBA]_0 = 0.5$ mg L^{-1}; $C_{PCN-U} = 100$ mg L^{-1}; $[S.A.]_0 = 10$ mM; and simulated solar irradiation.

catalysts to the PNBA solution in the presence of oxalic acid, at natural pH (ca. 4). Fig. 7 shows the PNBA concentration profile with irradiation time obtained with each material. As can be observed, the precursor used in the synthesis of g-C_3N_4 materials shows a slight influence on the photocatalytic performance of the materials for PNBA reduction. Specifically, the PCN-M material demonstrates a lower efficiency, possibly associated with a higher degree of layer stacking, as evidenced by the X-ray diagram (Fig. 1) and SEM micrographs provided (Fig. 2), which results in a material with a reduced surface area (Table 1). After the exfoliation treatment, a similar photocatalytic performance was detected for ECN-U and ECN-M, despite the differences observed in their respective surfaces areas (Table 1). On the contrary, the comparison of the kinetics obtained with the pristine and the exfoliated samples shows that the thermal exfoliation treatment might have a beneficial effect on the photocatalytic performance of the materials, as percentages of PNBA degradation are systematically higher with the exfoliated materials. Even though the exfoliation treatment of PCN-U and PCN-M results in a significant increase of the surface, unlike what has been reported in several oxidation processes [13], this property does not seem to be significant in the efficiency of photocatalytic reduction. Indeed, as displayed in Table 1, the surface areas of ENC-U and ECN-M are significantly different (448 and 77 m^2 g^{-1}, respectively) whereas both materials showed a similar photocatalytic performance for PNBA (Fig. 7). A plausible explanation for the beneficial effect induced by the thermal exfoliation should be the structural defects formed in the etching treatment, which can affect the rate of recombination of photogenerated charges [34]. As shown in the PL spectra (Fig. 4), a decrease in the radiative electron-hole recombination rate was detected in the exfoliated samples compared with the bulk materials, what indicates a higher lifetime of charge carriers in ECN-U and ECN-M caused by a decrease of the layer thickness of the carbon nitride structure observed in the X-ray diffraction and SEM micrographs [21].

Fig. 8 shows formation of PABA in the experiments performed with each catalyst. This compound, which has been described as the major intermediate in the degradation of PNBA [8], was detected in all the reactions driven with N_2 in the presence of sacrificial agents showing that, under these conditions, reduction plays an important role. It can be observed that PABA concentration increases in the early stages of the reaction to reach values close to 20% of the stoichiometric amount, and then a slight decrease is observed. This is a typical behaviour of a by-product that in turn suffers further reaction. This is in sharp contrast with observations with ZVI where nearly quantitative formation of

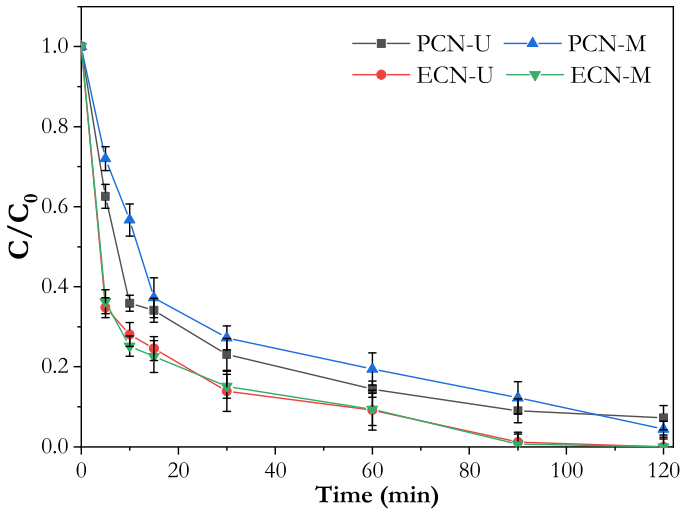

Fig. 7. Plot of the relative concentration of PNBA with irradiation time, in the presence of oxalic acid as sacrificial agent using different g-C_3N_4 photocatalysts. Experimental conditions: $[PNBA]_0 = 0.5$ mg L^{-1}; $C_{PCN-U} = 100$ mg L^{-1}; $[S.A.]_0 = 10$ mM; and simulated solar irradiation.

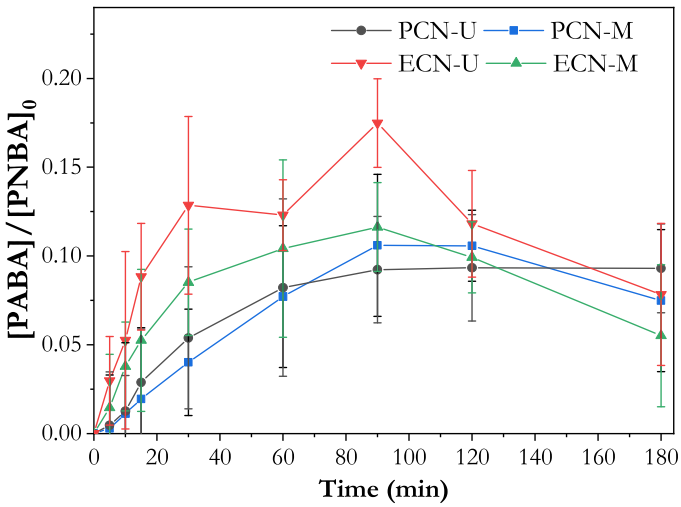

Fig. 8. Plot of the relative concentration of PABA, expressed as the ratio between the concentration of PABA and the initial concentration of PNBA. Experimental conditions: $[PNBA]_0 = 0.5$ mg L^{-1}; $[S.A.]_0 = 10$ mM (oxalic acid); $C_{g\text{-}C3N4} = 100$ mg L^{-1}; pH =3; N_2 atmosphere; and solar irradiation.

PABA acid was observed, what indicates by contrast to the reactions performed with g-C_3N_4, that the process is stopped at this product [8].

This might be explained by the existence of oxidative steps, as PABA is more easily oxidable than PNBA [8]. It has been recently reported that g-C_3N_4 is able to generate hydrogen peroxide even in the presence of low amounts of O_2 [35], and despite the reaction medium was deoxygenated with N_2, a low concentration of O_2 (in the range 0.5–1.0 mg L^{-1}) remained in the solution. Indeed, the formation of H_2O_2 (ca. 0.1 mM) was detected when ECN-U was irradiated in the presence of oxalic acid (10 mM). In addition, g-C_3N_4 and H_2O_2 have been demonstrated to have a strong synergetic effect in pollutants oxidation [36]. However, determining univocally that an oxidation step is occurring and the nature of the key reactive species requires further research.

4. Conclusions

g-C_3N_4 have been demonstrated as a promising photocatalyst for the reduction of PNBA in deaerated media when irradiated with simulated sunlight. Sacrificial electron donors are needed to carry out the process, being carboxylic acids the most efficient scavengers in the process, in particular oxalic acid. The pH has a significant impact on the photocatalytic reduction of PNBA, governed by the charge of the solid catalyst, PNBA, and the electron donors. Regarding the materials evaluated, there is a slight influence of the precursor used in the synthesis of g-C_3N_4, (urea or melamine) on the photocatalytic performance for PNBA reduction whereas the exfoliation treatment had a beneficial effect mainly ascribed to the lower recombination rate of the photogenerated charges in the resulting materials.

Nonetheless, further work is still needed in two main directions: a) gaining further insight into mechanistic aspects of the process to confirm the existence of combined reductive and oxidative steps and to determine which are the key species ruling the process, and b) optimizing the process under experimental conditions closer to real scenarios.

CRediT authorship contribution statement

Ana M Amat: Funding acquisition, Conceptualization. **Jorge Plaza:** Writing – original draft, Investigation, Conceptualization. **Rubén López-Timoner:** Writing – original draft, Investigation. **Antonio ArquesL:** Writing – review & editing, Supervision, Funding acquisition, Conceptualization. **Amaya Arencibia:** Methodology, Formal analysis, Conceptualization. **Maria José López-Muñoz:** Writing – review & editing, Supervision, Funding acquisition, Conceptualization.

Declaration of Competing Interest

The authors declare the following financial interests/personal relationships which may be considered as potential competing interests: All authors reports financial support was provided by European Commission. All authors reports financial support was provided by Spain Ministry of Science and Innovation. If there are other authors, they declare that they have no known competing financial interests or personal relationships that could have appeared to influence the work reported in this paper

Data availability

Data will be made available on request.

Acknowledgements

This work is dedicated to Prof. Santiago Esplugas for his retirement. Authors acknowledge the financial support of Spanish Ministerio de Ciencia e Innovación (PID2021-126400OB-C31, and PID2021-126400OB-C32, AquaEnAgri Project), Comunidad de Madrid (REMTAVARES Programme P2018/EMT-4341), European Union's Horizon 2020 research and innovation program under the Marie Skłodowska-Curie grant agreement No 101007578, SusWater Project, and TED2021-130994B-C32 (Ecotranseas) funded by European Union NextGenerationEU with the support of Ministerio de Ciencia e Innovación – Spanish Government.

Appendix A. Supporting information

Supplementary data associated with this article can be found in the online version at doi:10.1016/j.cattod.2024.114674.

References

[1] Q. Wang, W. Wei, Y. Gong, Q. Yu, Q. Li, J. Sun, Z. Yuan, Technologies for reducing sludge production in wastewater treatment plants: state of the art, Sci. Total Environ. 587–588 (2017) 510–521, https://doi.org/10.1016/J.SCITOTENV.2017.02.203.
[2] I. Oller, S. Malato, J.A. Sánchez-Pérez, Combination of advanced oxidation processes and biological treatments for wastewater decontamination—a review, Sci. Total Environ. 409 (2011) 4141–4166, https://doi.org/10.1016/J.SCITOTENV.2010.08.061.
[3] L. Rizzo, Addressing main challenges in the tertiary treatment of urban wastewater: are homogeneous photodriven AOPs the answer? Environ. Sci. (Camb. 8 (2022) 2145–2169, https://doi.org/10.1039/D2EW00146B.
[4] S. Zahmatkesh, A. Bokhari, M. Karimian, M.M.A. Zahra, M. Sillanpää, H. Panchal, A.J. Alrubaie, Y. Rezakhani, A comprehensive review of various approaches for treatment of tertiary wastewater with emerging contaminants: what do we know? Environ. Monit. Assess. 194 (2022) https://doi.org/10.1007/S10661-022-10503-Z.
[5] A. Giwa, A. Yusuf, H.A. Balogun, N.S. Sambudi, M.R. Bilad, I. Adeyemi, S. Chakraborty, S. Curcio, Recent advances in advanced oxidation processes for removal of contaminants from water: a comprehensive review, Process Saf. Environ. Prot. 146 (2021) 220–256, https://doi.org/10.1016/J.PSEP.2020.08.015.
[6] D.B. Miklos, C. Remy, M. Jekel, K.G. Linden, J.E. Drewes, U. Hübner, Evaluation of advanced oxidation processes for water and wastewater treatment – A critical review, Water Res. 139 (2018) 118–131, https://doi.org/10.1016/J.WATRES.2018.03.042.
[7] L. Santos-Juanes, S. García-Ballesteros, R.F. Vercher, A.M. Amat, A. Arques, Commercial steel wool used for Zero Valent Iron and as a source of dissolved iron in a combined red-ox process for pentachlorophenol degradation in tap water, Catal. Today 328 (2019) 252–258, https://doi.org/10.1016/J.CATTOD.2019.01.007.
[8] L. Santos-Juanes, F.S. García Einschlag, A.M. Amat, A. Arques, Combining ZVI reduction with photo-Fenton process for the removal of persistent pollutants, Chem. Eng. J. 310 (2017) 484–490, https://doi.org/10.1016/J.CEJ.2016.04.114.
[9] M.J. López-Muñoz, J. Aguado, A. Arencibia, R. Pascual, Mercury removal from aqueous solutions of HgCl2 by heterogeneous photocatalysis with TiO2, Appl. Catal. B 104 (2011) 220–228, https://doi.org/10.1016/J.APCATB.2011.03.029.
[10] F. Fu, D.D. Dionysiou, H. Liu, The use of zero-valent iron for groundwater remediation and wastewater treatment: a review, J. Hazard Mater. 267 (2014) 194–205, https://doi.org/10.1016/J.JHAZMAT.2013.12.062.

[11] J.A. Donadelli, L. Carlos, A. Arques, F.S. García Einschlag, Kinetic and mechanistic analysis of azo dyes decolorization by ZVI-assisted Fenton systems: pH-dependent shift in the contributions of reductive and oxidative transformation pathways, Appl. Catal. B 231 (2018) 51–61, https://doi.org/10.1016/J.APCATB.2018.02.057.
[12] J. Zhu, P. Xiao, H. Li, S.A.C. Carabineiro, Graphitic carbon nitride: synthesis, properties, and applications in catalysis, ACS Appl. Mater. Interfaces 6 (2014) 16449–16465, https://doi.org/10.1021/am502925j.
[13] J. Plaza, A. Arencibia, M.J. López-Muñoz, Optimization of thermal exfoliation of graphitic carbon nitride for methylparaben photocatalytic degradation under simulated solar radiation, J. Mater. Chem. A Mater. 11 (2023) 9922–9930, https://doi.org/10.1039/d3ta01109g.
[14] A. Al-Ahmed, Photocatalytic properties of graphitic carbon nitrides (g-C3N4) for sustainable green hydrogen production: recent advancement, Fuel 316 (2022) 123381, https://doi.org/10.1016/j.fuel.2022.123381.
[15] X. Zhang, P. Yang, g-C3N4 Nanosheet nanoarchitectonics: H2 generation and CO2 reduction, ChemNanoMat 9 (2023), https://doi.org/10.1002/CNMA.202300041.
[16] V. Hasija, P. Raizada, P. Singh, N. Verma, A.A.P. Khan, A. Singh, R. Selvasembian, S.Y. Kim, C.M. Hussain, V.H. Nguyen, Q.Van Le, Progress on the photocatalytic reduction of hexavalent Cr (VI) using engineered graphitic carbon nitride, Process Saf. Environ. Prot. 152 (2021) 663–678, https://doi.org/10.1016/J.PSEP.2021.06.042.
[17] S. Lu, L. Shen, X. Li, B. Yu, J. Ding, P. Gao, H. Zhang, Advances in the photocatalytic reduction functions of graphitic carbon nitride-based photocatalysts in environmental applications: a review, J. Clean. Prod. 378 (2022) 134589, https://doi.org/10.1016/J.JCLEPRO.2022.134589.
[18] I. Vallés, I. Sciscenko, M. Mora, P. Micó, A.M. Amat, L. Santos-Juanes, J. Moreno-Andrés, A. Arques, On the relevant role of iron complexation for the performance of photo-Fenton process at mild pH: role of ring substitution in phenolic ligand and interaction with halides, Appl. Catal. B 331 (2023) 122708, https://doi.org/10.1016/J.APCATB.2023.122708.
[19] R. López-Timoner, M. Mora, E. Zuriaga, J. Climent, L. Santos-Juanes, A.M. Amat, A. Arques, UVC-Assisted tertiary treatments for the removal of pollutants of emerging concern in real WWTP matrices, Page 882. 15, Water 2023 Vol. 15 (2023) 882, https://doi.org/10.3390/W15050882.
[20] Y. Kang, Y. Yang, L.C. Yin, X. Kang, G. Liu, H.M. Cheng, An amorphous carbon nitride photocatalyst with greatly extended visible-light-responsive range for photocatalytic hydrogen generation, Adv. Mater. 27 (2015) 4572–4577, https://doi.org/10.1002/adma.201501939.
[21] Y. Li, M.Q. Wang, S.J. Bao, S. Lu, M. Xu, D. Long, S. Pu, Tuning and thermal exfoliation graphene-like carbon nitride nanosheets for superior photocatalytic activity, Ceram. Int. 42 (2016) 18521–18528, https://doi.org/10.1016/J.CERAMINT.2016.08.190.
[22] Y. Zhang, Z. Huang, C.L. Dong, J. Shi, C. Cheng, X. Guan, S. Zong, B. Luo, Z. Cheng, D. Wei, Y. cheng Huang, S. Shen, L. Guo, Synergistic effect of nitrogen vacancy on ultrathin graphitic carbon nitride porous nanosheets for highly efficient photocatalytic H_2 evolution, Chem. Eng. J. 431 (2022) 134101, https://doi.org/10.1016/J.CEJ.2021.134101.
[23] G. Kesavan, S.M. Chen, Sonochemically exfoliated graphitic-carbon nitride for the electrochemical detection of flutamide in environmental samples, Diam. Relat. Mater. 108 (2020) 107975, https://doi.org/10.1016/J.DIAMOND.2020.107975.
[24] X. Li, H. Zhang, J. Huang, J. Luo, Z. Feng, X. Wang, Folded nano-porous graphene-like carbon nitride with significantly improved visible-light photocatalytic activity for dye degradation, Ceram. Int 43 (2017) 15785–15792, https://doi.org/10.1016/j.ceramint.2017.08.144.
[25] Y. Yuan, L. Zhang, J. Xing, M.I.B. Utama, X. Lu, K. Du, Y. Li, X. Hu, S. Wang, A. Genç, R. Dunin-Borkowski, J. Arbiol, Q. Xiong, High-yield synthesis and optical properties of g-C3N4, Nanoscale 7 (2015) 12343–12350, https://doi.org/10.1039/c5nr02905h.
[26] J. Xu, L. Zhang, R. Shi, Y. Zhu, Chemical exfoliation of graphitic carbon nitride for efficient heterogeneous photocatalysis, J. Mater. Chem. A Mater. 1 (2013) 14766–14772, https://doi.org/10.1039/c3ta13188b.
[27] C.H. Zhou, S.B. Cheng, J.L. Sun, H.M. Yin, K.L. Han, G.Z. He, Dynamics of OH formation in the photodissociation of o-nitrobenzoic acid at 295 and 355 nm, J. Phys. Chem. A 113 (2009) 4923–4929, https://doi.org/10.1021/JP900567U.
[28] A.M. Amat, A. Arques, S.H. Bossmann, A.M. Braun, S. Göb, M.A. Miranda, E. Oliveros, Oxidative degradation of 2,4-xylidine by photosensitization with 2,4,6-triphenylpyrylium: homogeneous and heterogeneous catalysis, Chemosphere 57 (2004) 1123–1130, https://doi.org/10.1016/J.CHEMOSPHERE.2004.08.029.
[29] Z. Teng, W. Cai, S. Liu, C. Wang, Q. Zhang, S. Chenliang, T. Ohno, Bandgap engineering of polymetric carbon nitride copolymerized by 2,5,8-triamino-tri-s-triazine (melem) and barbituric acid for efficient nonsacrificial photocatalytic H2O2 production, Appl. Catal. B 271 (2020) 118917, https://doi.org/10.1016/J.APCATB.2020.118917.
[30] S.K. Sharma, D. Chhimpa, I.K. Sharma, P.S. Verm, Electrochemical reduction of p-nitrobenzoic acid at glassy carbon and stainless steel (SS-316) electrode at different pH, Asian J. Chem. (2009) 3976–3980.
[31] M.E. Calvo, R.J. Candal, S.A. Bilmes, Photooxidation of organic mixtures on biased TiO_2 films, Environ. Sci. Technol. 35 (2001) 4132–4138, https://doi.org/10.1021/ES010613R.
[32] M. Fronczak, M. Krajewska, K. Demby, M. Bystrzejewski, Extraordinary adsorption of methyl blue onto sodium-doped graphitic carbon nitride, J. Phys. Chem. C. 121 (2017) 15756–15766, https://doi.org/10.1021/ACS.JPCC.7B03674.
[33] D.R. Lide, CRC handbook of chemistry and physics, (2001). ⟨https://books.google.com/books/about/CRC_Handbook_of_Chemistry_and_Physics_82.html?hl=es&id=Z68IswEACAAJ⟩ (accessed November 21, 2023).
[34] T.V. de Medeiros, A.O. Porto, H.A. Bicalho, J.C. González, R. Naccache, A.P. C. Teixeira, The effects of chemical and thermal exfoliation on the physico-chemical and optical properties of carbon nitrides, J. Mater. Chem. C. Mater. 9 (2021) 7622–7631, https://doi.org/10.1039/d1tc01734a.
[35] C. Liang, X.M. Wang, W. Liu, H.Y. Liu, D.W. Huang, Y.Z. Zhang, K.H. Zhang, L. S. Jiang, Y.Y. Jia, C.G. Niu, Functionalized graphitic carbon nitride based catalysts in solar-to-chemical conversion for hydrogen peroxide production, Chem. Eng. J. 466 (2023) 142931, https://doi.org/10.1016/j.cej.2023.142931.
[36] Q.L. Chen, Y.L. Liu, L.G. Tong, Enhanced visible light photocatalytic activity of g-C_3N_4 assisted by hydrogen peroxide, Mater. Res. Express 5 (2018) 046203, https://doi.org/10.1088/2053-1591/aab8c7.